ADVANCED MATERIALS TECHNOLOGIES
www.advmattechnol.de

Dynamic Interfacial Printing for Monodisperse Droplets and Polymeric Microparticles

Shenglong Liao, Yonglin He, Dingguan Wang, Libing Dong, Wenbin Du, and Yapei Wang**

Polymeric particles of micrometer size have attracted tremendous attention in the areas of controlled release,[1,2] biomedical imaging,[3,4] optoelectronics,[5] reinforcement materials,[6] and photonic crystals.[7] In addition to exploiting particles with diverse shapes, great efforts have been devoted to improving the degree of particle uniformity and regulating particle composition.[8,9] The precise control over uniformity and composition of polymer particles has led to a remarkable increase of repeatability and reliability in their valid application.[10,11] Traditional emulsion ways provide a facile and large-scale platform for converting polymers into solid particles, while polymer particles as a result of solidification of emulsion droplets always take the form of polydispersity.[12] The microfluidic technique appears to be the most powerful tool to produce monodisperse droplets with the size ranging from several to hundred micrometers, affording great promise for the generation of polymeric microparticles with high uniformity.[13–21] However, serious deformation of elastomeric microchannels by organic solvent is always raised on account of the swelling issue.[22–24] This intrinsic incompatibility restricts the use of many theta solvents for dissolving particular polymers. Microfluidic devices composed of silicon,[25] glass,[26–28] or perfluoropolyether[29,30] have come into being which exhibit effective solvent resistance. Yet their preparation routinely relies on time-consuming and sophisticated microfabrication processes.

The innovation of inkjet printing, e.g., Jetlab Printer,[31] provides a new platform for establishing droplets on demand, with droplet size closely constrained by the inner diameter of the nozzle. It is claimed that most solvents can be printed into uniform droplets by Jetlab Printer as its nozzle is made of glass. However, the printer is extremely expensive in comparison with microfluidic techniques and the inks should possess proper viscosity and surface tension though the printer affords great convenience to microengineering. Herein, we developed a dynamic interfacial printing (DIP) technique for preparing monodisperse droplets as well as polymeric microparticles. Different from the conventional inkjet printer with static nozzles, the DIP instrument has a dynamic nozzle periodically tapping an air–water interface. Similar to microfluidic devices, the droplets are formed due to interfacial shearing instead of piezoelectric pushing used in inkjet printing. DIP devices are free of photolithography and can be manually assembled within several minutes. It produces highly uniform polymeric microparticles with precise control over size in a wide range. In addition to cost effective preparation, the printing module made of Teflon and silica capillary tubes exhibits perfect compatibility with organic solvents and polymers.

Figure 1a illustrates the components and assembly of a typical DIP system. Polymer solution is injected by a programmable syringe pump into a water pool through a silica capillary tube connected with a gastight syringe via a Teflon tube. A vibration system including an electric vibrator and a function generator provides the driving force for vibrating the silica capillary tube at air–water interface. In a typical DIP process, the silica capillary tube anchored on the vibrator, acting like a dynamic nozzle, periodically goes up and down across an air–water interface (Figure 1b; Movie S1, Supporting Information). Along with the interfacial vibration, an oil phase is pumped out of the nozzle from the injection system into a water phase, which is sheared into a uniform droplet each time the nozzle leaves the interface. Without special statement, sodium lauryl sulfate (SDS) serving as a surfactant is added in the water phase in order to stabilize the oil droplets. As shown in Figure 1c,d, a model solvent of carbon tetrachloride (CCl_4) was printed into droplets with high degree of uniformity. At given flow rate and vibration frequency, the size of CCl_4 droplets is almost retained at a constant value (average diameter ≈31.8 μm, at flow rate of 0.06 μL min^{-1} and vibration frequency of 50 Hz). Statistical analysis reveals that the polydispersity index (PDI) of droplet diameters is as low as 4.4%. The DIP printed droplets render the possibility to serve as templates for preparing various polymeric microparticles. A volatile solvent of chloroform loaded with polymethylmethacrylate (PMMA) was printed into monodisperse droplets followed with the evaporation of chloroform. As shown in Figure 1e, complete removal of chloroform yielded solid PMMA particles with a narrow size distribution (Figure 1f).

To clarify the principle of droplet formation by DIP, the dynamic printing process was viewed and captured on a high-speed camera. As played in Movie S2 (Supporting Information) (recording frame rates, 2000 fps), the droplet outflows from the nozzle and grows bigger below the air–water interface. Each time the nozzle goes up above the interface, the droplet is sheared by the interface and escapes from the nozzle. The

S. Liao, Y. He, D. Wang, L. Dong, Prof. Y. Wang
Department of Chemistry
Renmin University of China
Beijing 100872, China
E-mail: yapeiwang@ruc.edu.cn
L. Dong, Prof. W. Du
State Key Laboratory of Microbial Resources
Institute of Microbiology
Chinese Academy of Sciences
Beijing 100101, China
E-mail: wenbin@im.ac.cn

DOI: 10.1002/admt.201600021

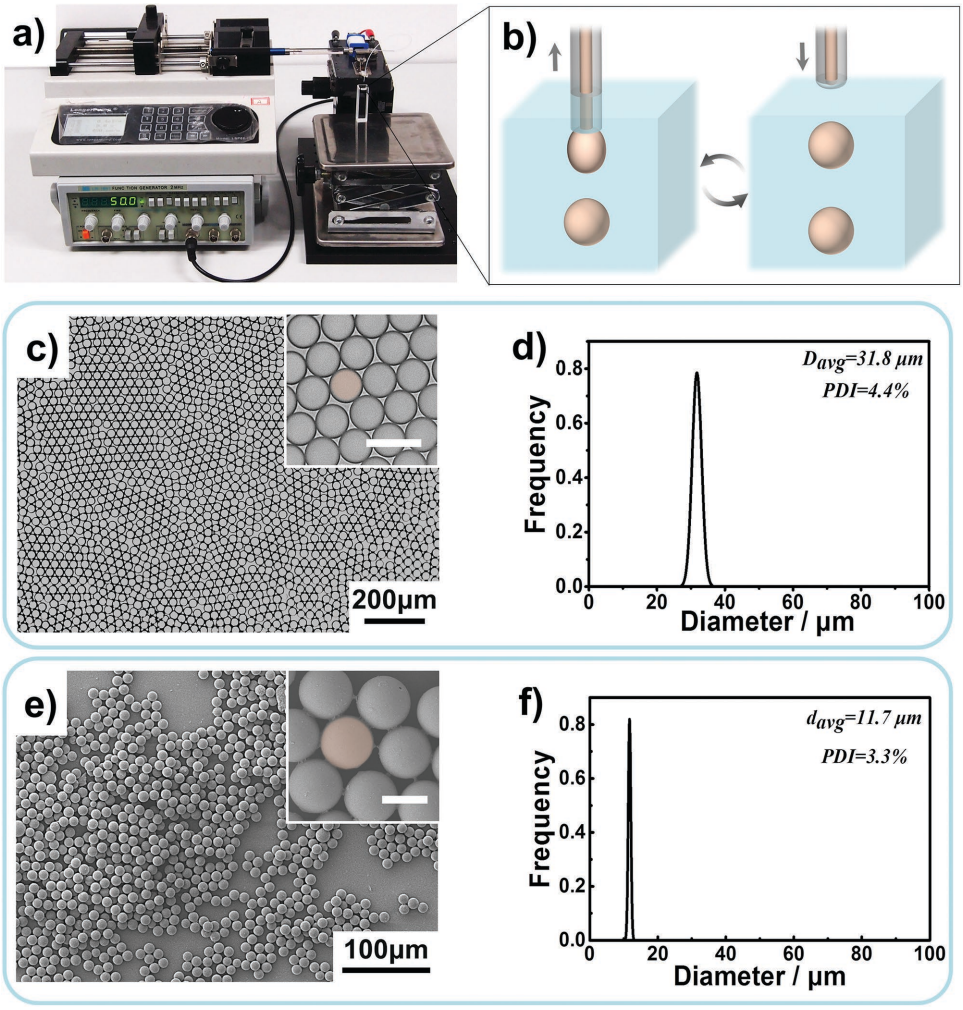

Figure 1. Overview of dynamic interfacial printing (DIP) system. a) An experimental setup including a Teflon tube inserted with a silica capillary tube, a glass syringe driven by pump, a function generator, and an electric vibrator. b) A schematic illustration of the formation of droplets by DIP. c) Optical microscopic image of CCl_4 droplets in water with addition of SDS (5.0 mg mL^{-1}) under large-field view, generated by DIP at a flow rate of 0.06 μL min^{-1} and printing frequency of 50 Hz. The inset is a magnified image with scale bar of 50 μm. d) The size distribution plot of droplets generated at the same conditions as (c). 1000 droplets were measured by Photoshop software. e) SEM image of PMMA particles as a result of solidification of droplets by printing PMMA solution (0.5 wt% in chloroform) at a flow rate of 0.40 μL min^{-1} and vibration frequency of 50 Hz. The inset is a magnified photograph with scale bar of 10 μm. f) The size distribution of PMMA particles prepared under the same conditions as (e). 500 PMMA microparticles were measured by Photoshop software.

droplets settle down or float up in the water pool if the solvent density is higher (e.g., CCl_4, see Movie S2, Supporting Information) or lower (e.g., *n*-octane, see Movie S4, Supporting Information) than the density of water. There are two key forces in determining the formation of oil droplets: (1) a strong enough capillary force that can hold the oil droplet moving together with the nozzle at high speed and acceleration below the interface; (2) a shearing force that can cut off the pendant oil droplet from the nozzle near the interface.

To examine if the capillary force provided by the silica nozzle is strong enough to hold the oil droplet before reaching the interface, all forces acting upon the droplet are identified. As illustrated in **Figure 2**a, when the nozzle moves upward, the droplet receives a capillary force (F_c) and a buoyancy force (F_b) both toward the moving direction. The gravity (G), injection pressure force (F_p), and Stokes drag force (F_v) are the dragging forces that hinder the motion of droplet. According to Newton's Second Law, the total force as the sum of above five forces is equal to mass (m) multiplied by acceleration (a). Therefore, the capillary force (F_c) can be calculated by the following equation

$$F_c = G + F_p + F_v + ma - F_b \quad (1)$$

Based on the analysis of movies captured on the high speed camera, parameters relevant to the motion of nozzle can be figured out. Two critical parameters of velocity and acceleration, which decide the Stokes force and the total force respectively, change periodically as function of nozzle position or vibration time in a typical harmonic motion driven by an AC (Figure S1, Supporting Information). Accordingly, as discussed in detail in Note S2 (Supporting Information), the total force and Stokes drag force change dynamically in the whole vibration process.

Adv. Mater. Technol. **2016**,
DOI: 10.1002/admt.201600021

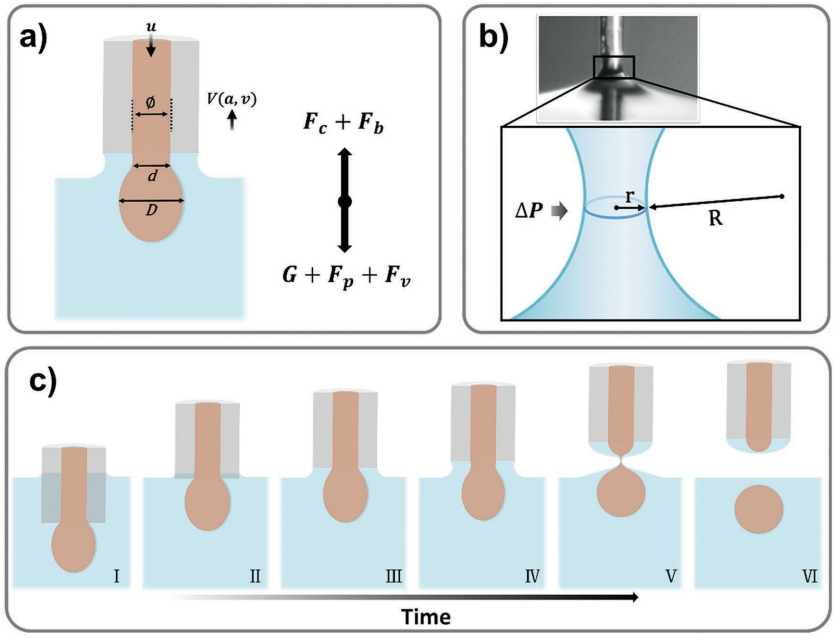

Figure 2. Schematic illustration of DIP principle. a) Schemes of DIP model (left) and force analysis (right) of droplet pulled by the silica nozzle underwater. The left graph contains the following parameters – the velocity of fluid: *u*; the inner diameter of the silica capillary: ∅; the diameter of the neck part between droplet and nozzle: *d*; the diameter of the pendant drop: *D*; the velocity of nozzle: *v*, and the acceleration: *a*. b) The optical photograph captured on a high speed camera at a frame speed of 6000 fps, showing the moment at which interfacial shearing happens to the droplet. c) The profile of droplet at different stages in a half period of nozzle vibration.

Gravity as well as buoyancy forces are also variable at different positions due to the change of droplet volume. Regardless of the change of injection pressure force, the dynamic capillary force needed to balance the motion of droplet with nozzle from the lowest position to equilibrium location (stage II as presented in Note S2, Supporting Information) are estimated in Figure S2 (Supporting Information). A capillary force of 4.93×10^{-8} N appears at the equilibrium state where the velocity reaches its maximum. As explained in Note S2 (Supporting Information), this value is regarded as the maximum capillary force in the whole vibration process. Remarkably, it is smaller than the theoretical maximum capillary force about 3.44×10^{-7} N provided by the nozzle, indicating that the capillary force is strong enough to hold the oil droplet moving at high speed and high acceleration below the air–water interface.

A shearing force should exist in the vicinity of air–water interface that is able to cut off the droplet. To find out the reason for the formation of shearing force, the dynamic motion of the silica nozzle going across the interface was precisely monitored on a camera with higher speed of 6000 fps (Movie S3, Supporting Information). Great insights reveal that the air–water interface is gradually deformed into a saddle shape when the end of nozzle rises above the horizontal plane (Figure 2b). As a result of surface tension, this interfacial deformation causes a pressure difference (ΔP) between the air and water, which is determined by Young–Laplace equation

$$\Delta P = \gamma_{l,g} \times \left(\frac{1}{r} - \frac{1}{R}\right) \quad (2)$$

Where $\gamma_{l,g}$ is the interfacial tension between water phase and air; r is the radius of inner neck; and R is the radius of outline curvature. Obviously, r is much smaller than R. Therefore, the direction of the Young–Laplace pressure, which represents the nature of the shearing force, points toward the water surface. As the droplet moves up further, the diameter of oil neck region, d, becomes smaller leading to weaker capillary force. Once the capillary force drops to a low value ($F_{c,min}$), it can no longer hold the pendant oil droplet and the droplet leaves the nozzle. Since the minimum capillary force ($F_{c,min}$) can be learned from Equation (1), the critical diameter (d_{min}) of the breaking neck can be worked out by the following Equation (3), where $\gamma_{o,w}$ is the interfacial tension between oil phase and water phase. For example, in the case of printing CCl_4 droplets at a flow rate of 1.00 µL min^{-1} and vibration frequency of 50 Hz, the minimum diameter dmin is 4.0 µm

$$F_{c,min} = \pi d_{min} \times \gamma_{o,w} \quad (3)$$

The droplet size can be readily tailored by changing the flow rate (Q) or the vibration frequency (f). As presented in Equation (4), the volume (V) of a printed oil droplet obeys a function of the flow rate (Q) and the vibration frequency (f). Therefore, the droplet diameter (D) can be worked out in Equation (5)

$$V = Q/f \quad (4)$$

$$D = \sqrt[3]{6Q/(\pi f)} \quad (5)$$

As shown in **Figure 3**a–c, keeping the vibration frequency unchanged, CCl_4 solutions can be printed into monodisperse droplets with a range of sizes at different flow rates (Figures S3 and S4, Supporting Information). On the other hand, at a constant flow rate, the droplet size can also be regulated by changing the vibration frequency (Figure 3d–f; Figures S5 and S6, Supporting Information). The relationships between droplet size and flow rate or vibration frequency were established (Figure 3g,h). The droplet volume as measured based on the analysis of microscope images is highly proportional to the flow rate or the vibration period, matching the theoretical results as predicted by Equation (4). Moreover, the diameters of droplets generated at different conditions are consistent with the theoretical results calculated by Equation (5) (Tables S1 and S2, Supporting Information). It is envisioned that droplets with a wide range of sizes can be printed out by adjusting the flow rate and the vibration frequency, even to nanometer level if ultrahigh frequency is applied.

To improve the throughput of droplets, an augmented printer with multiple nozzles assembled in parallel in one Teflon tube was developed (Movie S5, Supporting Information). Similar to one-nozzle printing, the size of droplets is faithfully confined to flow rate and vibration frequency. Additionally, it

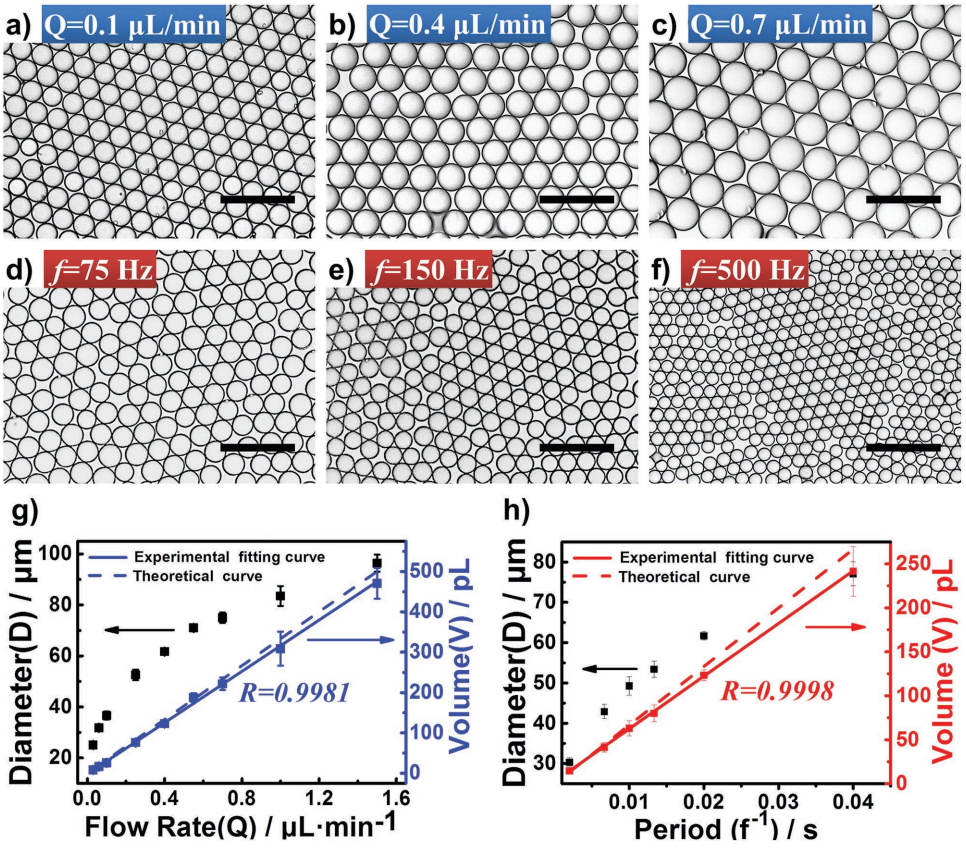

Figure 3. Tuning the droplet size by changing flow rate and vibration frequency. a–c) CCl_4 droplets with different sizes, produced with the same vibration frequency of 50 Hz but different flow rates. The flow rate is 0.10, 0.40, and 0.70 μL min^{-1} from (a) to (c), respectively. d–f) CCl_4 droplets with different sizes, produced at the same flow rate of 0.40 μL min^{-1} and different vibration frequency. The vibration frequency is 75, 150, and 500 Hz from (d) to (f), respectively. g) The plot of the droplet size as a function of flow rate. h) The plot of the droplet size as a function of vibration period. In (g) and (h), the full line refers to a linear fitting plot of experimental results and the dashed line is a calculation curve according to Equation (4). Scale bar: 200 μm.

also varies inversely with the number of channels (N) as presented in Equation (6)

$$V = Q/(Nf) \tag{6}$$

This Equation was validated with one-, two-, and four-nozzle printings (Figure S7, Supporting Information). For printer with multiple nozzles, the solution delivered from the Teflon tube was assigned to each nozzle. As a result, the droplet volume as well as the size decrease with the use of multiple nozzles at given flow rate and vibration frequency. Intending to obtain droplets with a specific size, the flow rate of two-nozzle and four-nozzle printers in comparison with one-nozzle printer has to be doubled or quadrupled, respectively (Figure S8, Supporting Information). Correspondingly, number of droplets produced in a finite period can be successfully increased.

In terms of high compatibility, the DIP printer composed of only silica and Teflon is able to endure almost all the organic solvents and surfactants in water phase. Several solvents that are immiscible with water, such as toluene, *n*-octane, tetrachloromethane, chloroform, and chlorobenzene have been attempted. These solvents can all be printed into monodisperse droplets with precise control over the size. The droplets made of them at the same conditions can not be distinguished except the different density (Figure S9, Supporting Information). In addition to SDS, the use of another common surfactant of polyvinyl alcohol can also lead to monodisperse and stable oil droplets. Yet the droplets printed into aqueous solution having cetyl trimethyl ammonium bromide (CTAB) are not uniform (Figure S10c, Supporting Information). This exceptional printing is attributed to the adhesion of CTAB on the outer surface of silica nozzle due to the electrostatic interaction between cation of CTAB and hydroxyl moieties on silica surface (Figure S11, Supporting Information). As a consequence, the oil droplets are able to wet the outer surface of silica nozzle which causes an irregular interfacial shearing. The adhesion of CTAB could be hampered by assembling a layer of 3-aminopropyltrimethoxysilane with the ability of repulsing CTAB on the silica nozzle. Again, oil phase becomes nonwetting to the silica nozzle and can be sheared into monodisperse droplets (Figure S10d, Supporting Information).

Monodisperse droplets made of diverse solvents by the DIP technique afford a great platform for preparing polymeric microparticles with a high degree of uniformity. In principle, polymers dissolved in oil droplets can be condensed into solid particles upon the removal of solvents. Particle size relies on the polymer concentration as well as the droplet size. Taking polystyrene (PS) as an example, its chloroform solution can

DOI: 10.1002/admt.201600021

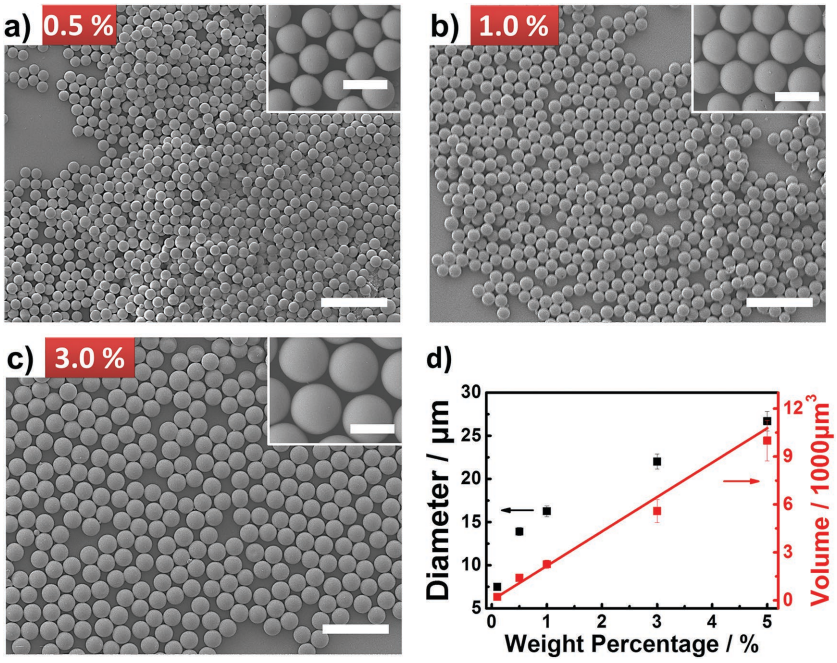

Figure 4. SEM images of polystyrene particles solidified from chloroform droplets dissolving polystyrene with different concentrations: a) 0.5 wt%, b) 1.0 wt%, c) 3.0 wt%. The flow rate and vibration frequency of DIP are 0.40 µL min^{-1} and 50 Hz, respectively. Scale bars: 100 µm. The scale bars of the inset images are 20 µm. d) The droplet volume and particle size as function of polystyrene concentration in chloroform.

be readily printed into droplets and turned into microparticles upon the evaporation of chloroform. At the given flow rate and vibration frequency, the droplet size was not affected by polymer concentration, while lower concentration led to smaller polystyrene particles (**Figure 4**a–c). The particle volume is theoretically proportional to the polymer concentration, which is verified by multiple practices at different concentrations (Figure 4d). It is worth noting that many other polymers can be printed into solid particles by the DIP technique. As exemplified in Figure S12 (Supporting Information), biodegradable polymers like polylactic acid and polycarbonate, and block copolymers such as polystyrene-polymethyl methacrylate and polymethyl methacrylate-polyacrylonitrile have been successfully converted into microparticles.

To realize its full potential, DIP was extended to prepare polymeric microparticles with complicated morphologies. Three examples were presented, including elongated particles, particles with patchy surfaces, and porous particles (**Figure 5**). They have always been considered as star building blocks for colloid assembly and functional materials.[32–36] Elongated particles were attained by stretching polycaprolactone (PCL) particles that have been prepared already based on DIP (Figure 5a). Notably, DIP promised high degree of uniformity not only to spherical particles but also elongated particles. Patchy particles were formed based on the phase separation within a blend of PS and PMMA. Droplets dissolving two free polymers of PS and PMMA were allowed to be printed and solidified. Macrophase separation between PS and PMMA drives one polymer to migrate onto the particle surface, although we have not yet recognized which polymer is pushed out. Porous particles were synthesized based on in situ polymerization within droplets. A photocurable monomer having three active groups (Triacrylate) was loaded in droplets which can be cross-linked into a gel together with solvents under UV irradiation.[37] Porous morphology is a result of the complete removal of solvents. These examples are opening three possibilities: (1) DIP printed particles can be re-shaped. Shape-specific particles with high uniformity may facilitate the accurate understanding of shape effect in biological application since the particle shape has great effect to cellular interaction.[38] (2) Multiple components can be loaded in particles. Based on phase separation,

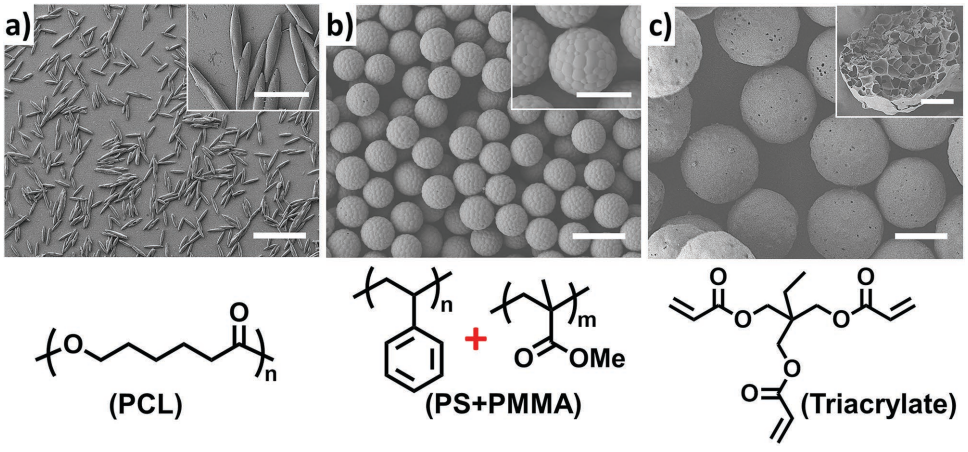

Figure 5. Preparation of polymeric microparticles with complicated morphology based on the DIP technique. SEM images of a) Elongated PCL particles with Scale bar of 200 µm. Scale bar of inset image is 100 µm; b) patchy particles of PS and PMMA blend with Scale bar of 20 µm. Scale bar of inset image is 10 µm; c) Porous polyacrylate particles with Scale bar of 20 µm. Scale bar of inset image is 10 µm. Triacrylate concentration in chloroform is 2.0 wt%.

Table 1. A Comparison of DIP method with traditional methods for generating monodisperse droplets.[9]

Microfabrication ways	Membrane emulsification	Microchannel array devices	Microfluidic devices	Inkjet printer[31]	DIP (4 nozzles)
PDI	10%–20%	<5%	<3%	<1%	<5%
Droplet diameter	0.1–1000 μm	1–1000 μm	10–1000 μm	20–1000 μm	20–1000 μm
Cost	Expensive	Expensive	Moderate	Very expensive	Cheap
Time for device fabrication	Several weeks	Several days	Several hours to days	–	<10 min
Compatibility	Good	Sensitive to organic solvents	Commonly sensitive to solvents	Good	Good
Efficiency [Number s^{-1}]	$<10^{15}$	$<5 \times 10^5$	$<2 \times 10^4$	$<5 \times 10^4$	$<2 \times 10^3$

uniform microparticles with other topologies, including dumbbell, core-shell, onion, are anticipated. (3) DIP droplets can serve as microreactors. In addition to photopolymerization, other chemical or biological reactions may be involved in the droplets. For example, sequencing or amplification of nucleic acid in the size-specific microdroplets has great potential for polymerase chain reaction (PCR) application.

In summary, we described a paradigm, simple, and low-cost DIP technique for preparing monodisperse droplets and uniform polymeric microparticles. Generation of droplets happens at an air–water interface based on an interfacial shearing. The method is like a combination of microfluidic flowing with periodical printing, affording great convenience to turn solutions into droplets. We provided a comparison of the DIP technique with other methods for generating liquid droplets (**Table 1**). Overall, DIP technique is most cost effective and generally applicable. The DIP printer could be rapidly built up with the use of readily available components. Unlike the most common polydimethylsiloxane-based microfluidic devices, the pipeline of DIP system endures almost all the organic solvents. In addition to preparing oil-in-water type of droplets, DIP technique can be principally extended to other combinations containing two or more immiscible phases, e.g., printing water into oil, air into water, water into water, or oil into oil. Convenient insights at various interfaces or within droplets are promised at macroscopic level. It is also believed that enclosing many other functional excipients in polymeric particles may broaden the range of materials with spatiotemporal functions. Great efforts have been devoted to integrating multiple nozzles in the DIP system for improving the throughput of droplets. Moreover, the development of high-level printers able to integrate multiple components in one droplet is undergoing. It is anticipated that some challengeable studies will be possibly launched based on the DIP technique.

Supporting Information

Supporting Information is available from the Wiley Online Library or from the author.

Acknowledgements

This work was financially supported by the National Natural Science Foundation of China (Grants Nos. 51373197, 21422407, 21205134, 31470221), the Program for New Century Excellent Talents in University (NCET-12-0530), and the Strategic Priority Research Program of the Chinese Academy of Sciences (XDB15040102).

Received: February 9, 2016
Revised: February 17, 2016
Published online:

[1] W.-L. Chiang, C.-J. Ke, Z.-X. Liao, S.-Y. Chen, F.-R. Chen, C.-Y. Tsai, Y. Xia, H.-W. Sung, *Small* **2012**, *8*, 3584.
[2] S.-H. Kim, J. W. Kim, D.-H. Kim, S.-H. Han, F. A. Weitz, *Small* **2013**, *9*, 124.
[3] S. Biswas, X. Wang, A. R. Morales, H.-Y. Ahn, K. D. Belfield, *Biomacromolecules* **2011**, *12*, 441.
[4] K. M. Au, Z. Lu, S. J. Matcher, S. P. Armes, *Biomaterials* **2013**, *34*, 8925.
[5] D. A. Kunz, J. Schmid, P. Feicht, J. Erath, A. Fery, J. Breu, *ACS Nano* **2013**, *7*, 4275.
[6] M. R. B. Mermet-Guyennet, J. G. de Castro, H. S. Varol, M. Habibi, B. Hosseinkhani, N. Martzel, R. Sprik, M. M. Denn, A. Zaccone, S. H. Parekh, D. Bonn, *Polymer* **2015**, *73*, 170.
[7] Y. Zhang, B. Dong, A. Chen, X. Liu, L. Shi, J. Zi, *Adv. Mater.* **2015**, *27*, 4719.
[8] W. Wang, M. Zhang, L. Chu, *Acc. Chem. Res.* **2014**, *47*, 373.
[9] G. T. Vladisavljević, I. Kobayashi, M. Nakajima, *Microfluid. Nanofluid.* **2012**, *13*, 151.
[10] J. Lee, P. W. Bisso, R. L. Srinivas, J. J. Kim, A. J. Swiston, P. S. Doyle, *Nat. Mater.* **2014**, *13*, 524.
[11] J.-Y. Wang, Y. Wang, S. Sheiko, D. E. Betts, J. M. DeSimone, *J. Am. Chem. Soc.* **2012**, *134*, 5801.
[12] X. Huang, R. Fang, D. Wang, J. Wang, H. Xu, Y. Wang, X. Zhang, *Small* **2015**, *11*, 1537.
[13] Q. Xu, M. Hashimoto, T. T. Dang, T. Hoare, D. S. Kohane, G. M. Whitesides, R. Langer, D. G. Anderson, *Small* **2009**, *13*, 1575.
[14] A. N. Mitropoulos, G. Perotto, S. Kim, B. Marelli, D. L. Kaplan, F. G. Omenetto, *Adv. Mater.* **2014**, *26*, 1105.
[15] D. Liu, S. Cito, Y. Zhang, C. Wang, T. M. Sikanen, H. A. Santos, *Adv. Mater.* **2015**, *27*, 2298.
[16] J. Wei, X. Ju, X. Zou, R. Xie, W. Wang, Y. Liu, L. Chu, *Adv. Funct. Mater.* **2014**, *24*, 3312.
[17] L. Zhang, Q. Feng, J. Wang, J. Sun, X. Shi, X. Jiang, *Angew. Chem. Int. Ed.* **2015**, *54*, 1.
[18] S. L. Anna, N. Bontoux, H. A. Stone, *Appl. Phys. Lett.* **2003**, *82*, 364.
[19] R. K. Shah, H. C. Shum, A. C. Rowat, D. Lee, J. J. Agresti, A. S. Utada, L. Chu, J. Kim, A. F. Nieves, C. J. Martinez, D. A. Weitz, *Mater. Today* **2008**, *11*, 18.
[20] S. Xu, Z. Nie, M. Seo, P. Lewis, E. Kumacheva, H. A. Stone, P. Garstecki, D. B. Weibel, I. Gitlin, G. M. Whitesides, *Angew. Chem. Int. Ed.* **2005**, *44*, 724.

[21] J. Cui, W. Zhu, N. Gao, J. Li, H. Yang, Y. Jiang, P. Seidel, B. J. Ravoo, G. Li, *Angew. Chem. Int. Ed.* **2014**, *53*, 3844.
[22] G. M. Whitesides, *Nature* **2006**, *442*, 368.
[23] J. N. Lee, C. Park, G. M. Whitesides, *Anal. Chem.* **2003**, *75*, 6544.
[24] M. W. Toepke, D. J. Beebe, *Lab Chip* **2006**, *7*, 1484.
[25] I. Kobayashi, S. Mukataka, M. Nakajima, *Langmuir* **2005**, *21*, 7629.
[26] Z. Meng, W. Wang, X. Liang, W. Zheng, N. Deng, R. Xie, X. Ju, Z. Liu, L. Chu, *Lab Chip* **2015**, *49*, 6129.
[27] D. Chen, W. Du, Y. Liu, W. Liu, A. Kuznetsov, F. E. Mendez, L. H. Philipson, R. F. Ismagilov, *Proc. Natl. Acad. Sci. USA* **2008**, *105*, 16843.
[28] A. S. Utada, E. Lorenceau, D. R. Link, P. D. Kaplan, H. A. Stone, D. A. Weitz, *Science* **2005**, *308*, 537.
[29] J. P. Rolland, R. M. V. Dam, D. A. Schorzman, S. R. Quake, J. M. DeSimone, *J. Am. Chem. Soc.* **2004**, *126*, 2322.
[30] K. W. Bong, J. Lee, P. S. Doyle, *Lab Chip* **2014**, *14*, 4680.
[31] Parameters for Jetlab and inkjet printers summarized in Table 1 are provided by http://www.rd-mv.com and http://www.microfab.com.
[32] X. Huang, Q. Qian, X. Zhang, W. Du, H. Xu, Y. Wang, *Part. Part. Syst. Char.* **2013**, *30*, 235.
[33] Y. Wang, Y. Wang, D. R. Breed, V. N. Manoharan, L. Feng, A. D. Hollingsworth, M. Weck, D. J. Pine, *Nature* **2012**, *491*, 51.
[34] Q. Chen, S. C. Bae, S. Granick, *Nature* **2011**, *469*, 381.
[35] Q. Qian, X. Huang, X. Zhang, Z. Xie, Y. Wang, *Angew. Chem. Int. Ed.* **2013**, *52*, 10623.
[36] J. Wang, J. Zhao, Y. Li, M. Yang, Y. Zhang, J. Zhang, Z. Sun, Y. Wang, *ACS Macro Lett.* **2015**, *4*, 392.
[37] X. Zhang, D. Ji, T. Lei, B. Zhao, K. Song, W. Hu, J. Wang, J. Pei, Y. Wang, *J. Mater. Chem.* **2013**, *1*, 10607.
[38] J. A. Champion, S. Mitragotri, *Proc. Natl. Acad. Sci. USA* **2006**, *103*, 4930.